AGU PUBLICATIONS

JGR

Journal of Geophysical Research: Space Physics

RESEARCH ARTICLE

10.1002/2014JA020790

**Key Points:**
- Geomagnetic-geographical axes offset is crucial for *Ne* longitudinal difference
- Solar illumination is important for background longitudinal pattern of *Ne*
- Migrating tides can enhance the difference by 15% over North America

**Correspondence to:**
H. Wang,
h.wang@whu.edu.cn

**Citation:**
Wang, H., A. J. Ridley, and J. Zhu (2015), Theoretical study of zonal differences of electron density at midlatitudes with GITM simulation, *J. Geophys. Res. Space Physics*, *120*, 2951–2966, doi:10.1002/2014JA020790.

Received 3 NOV 2014
Accepted 27 FEB 2015
Accepted article online 3 MAR 2015
Published online 1 APR 2015

# Theoretical study of zonal differences of electron density at midlatitudes with GITM simulation

**Hui Wang[1,2], Aaron J. Ridley[2], and Jie Zhu[2]**

[1]Department of Space Physics, School of Electronic Information, Wuhan University, Wuhan, China, [2]Department of Atmospheric, Oceanic, and Space Sciences, University of Michigan, Ann Arbor, Michigan, USA

**Abstract** This study investigated various physical processes responsible for the longitudinal modulation of electron density (*Ne*) at midlatitudes by employing the global ionosphere-thermosphere model (GITM). The good agreements between GITM outputs and CHAMP observations indicate that the model is a suitable tool to perform the theoretical study. Nine runs were carried out to determine the effects from geomagnetic field geometry, zonal wind, meridional wind, high-latitude activity, migrating tides from the lower atmosphere, and solar illumination in quantitative ways. Distinct features were discussed as follows. It was crucial that the geomagnetic and geographical axes were offset for the development of the longitudinal difference of *Ne*. The zonal wind contributes to about 80% of the fraction of the observed longitudinal dependence of *Ne*. The meridional wind effect is out of phase with the zonal wind over North America and Southern Ocean regions, which trims the fraction of the longitudinal difference to 65%. Over the South Pacific Ocean, the nighttime *Ne* maintains at a higher level because of in-phase effects from both zonal and meridional winds. The solar illumination was important in the formation of the background longitudinal pattern of the electron density. The migrating tide from the lower atmosphere could enhance the longitudinal difference of *Ne* by 15% over North America. Enhanced activities at high latitudes could alter the longitudinal pattern of *Ne* by transporting thermospheric composition disturbances to midlatitudes.

## 1. Introduction

The electron density at midlatitudes shows zonal (or longitudinal) variation, which tends to be explained by vertical drift effects caused by the zonal wind [e.g., *Zhang et al.*, 2011, 2012; *Zhao et al.*, 2013; *Xu et al.*, 2013; *Luan and Dou*, 2013; H. Wang et al., Interpretation of longitudinal pattern in the electron density at mid latitudes: CHAMP observation and global ionosphere-thermosphere model (GITM) simulation, submitted to *Chinese Science Bulletin*, 2015]. With the magnetic declination, the zonal wind can contribute to the plasma velocity in the geomagnetic field direction. Subsequently, the plasma are pushed down (or lifted up) the magnetic field lines to regions of higher (or lower) density molecular species, allowing more (or less) charge exchange to occur, which drives stronger (or weaker) chemical recombination rates, such that the peak density and the altitude of the peak are both lowered (or increased). As the magnetic declination angle shows a distinct zonal variation, electric densities vary significantly with longitude. *Zhang et al.* [2011] have reported a zonal difference in total electron content (TEC) over the United States in September 2005 with higher density in the east (60°W–80°W) than in the west (110°W–130°W) and vice versa in the morning TEC. Their work was based on observational data from GPS ground receivers in North America. The research results from *Zhang et al.* [2012] based on the long-term electron density data from the incoherent scatter radar at Millstone Hill from 1978 to 2011 and the zonal winds measured by the local FPI (Fabry-Perot Interferometer) during 1989 to 2001 have shown good correlation between the west-east electron density difference ratio and the zonal wind, further supporting the zonal wind effect. *Zhao et al.* [2013] have found that the morning (evening) peak electron density (NmF2) in the far east regions is larger (smaller) at 70°E than at 140°E. *Xu et al.* [2013] have reported west-east differences of TEC over North America (120°W, 70°W), South America (80°W, 50°W), and Southern Ocean (110°E, 180°E). *Luan and Dou* [2013] have found that the longitudinal variation in the evening electron density at southern midlatitudes, based on COSMIC satellite observations, are generally consistent with zonal wind effects. All these reported longitudinal differences are similar to the global maps presented from CHAMP electron density data. H. Wang et al. (submitted manuscript, 2015) have found that longitudinal

differences in *Ne* exhibit obvious interhemispheric and west-east hemispheric asymmetries, with larger amplitudes in the south than in the north and over the North American sector than the European-Asian sector. They also showed that the longitudinal differences in *Ne* are independent of season and solar activity level.

The longitudinal difference of the midlatitudinal electron density has been decomposed into nonmigrating tidal components [e.g., *Xiong and Lühr*, 2014; H. Wang et al., submitted manuscript, 2015]. The nonmigrating tides DE1, DW3, and SPW2 (D0, DW2, and SPW1) were shown to be responsible for the longitudinal and diurnal variations of *Ne* in the Northern (Southern) Hemisphere at solar maximum and medium conditions (H. Wang et al., submitted manuscript, 2015). By using global ionosphere-thermosphere model (GITM) simulations, H. Wang et al. (submitted manuscript, 2015) have advanced the idea that the nonmigrating tides originate from in situ ion-neutral coupling processes through the zonal wind-magnetic field mechanism rather than being propagated upward from the lower atmosphere.

The study reported here is a follow on work of H. Wang et al. (submitted manuscript, 2015), focusing on relative contributions to the longitudinal modulation of *Ne* by various physical processes. In particular, effects from geomagnetic field geometry, meridional wind, solar ionization, high-latitude electric field, and migrating tides from the lower atmosphere were investigated. *Zhang et al.* [2012] have assumed that the effect of the meridional wind in the North American sector was insignificant. However, *Luan and Dou* [2013] have argued that in the southern nighttime region, the meridional wind has a comparable effect on the electron density as the zonal wind. Thus, it can also affect the longitudinal locations of the maximum and minimum *Ne*. Further studies are necessary to understand the meridional wind effect for all local times across the globe. So far, few studies have quantitatively addressed the impact of solar illumination, high-latitude activity, and migrating tides from the lower atmosphere on the longitudinal difference of *Ne*.

For this purpose, the global ionosphere-thermosphere model is employed to perform the investigation. By using a globally coupled model, various interdependent physical processes can be separated, so an understanding of their relative contributions could be determined. Before the model is used to perform the evaluation, CHAMP satellite observations are utilized to evaluate the model's performance.

## 2. GITM Model

The global ionosphere-thermosphere model (GITM), developed at University of Michigan, is a three-dimensional model that simulates the ionosphere and thermosphere. A complete description of the model can be found in *Ridley et al.* [2006]. The model solves the continuity, momentum, and energy equations in the thermosphere and ionosphere with realistic source terms. The ion momentum equation is solved by considering the pressure gradients, gravity, neutral winds, and electric fields. GITM is driven by the high-latitude electric field [*Weimer*, 2005], auroral particle precipitation [*Fuller-Rowell and Evans*, 1987], solar EUV, and tides (global-scale wave model, GSWM) at the low boundary [*Hagan et al.*, 1999]. GITM is initiated by using MSIS (Mass-Spectrometer-Incoherent-Scatter) [*Hedin*, 1991] and IRI (International Reference Ionosphere) [*Bilitza*, 2001] neutral and ion densities and temperatures. The magnetic topology can be described either by the dipole field or the International Geomagnetic Reference Field (IGRF) [*Maus et al.*, 2005].

For this study, GITM is run with a resolution of 1° latitude by 5° longitude and with a stretched altitude, resolving the vertical scales with approximately one third of a scale height. It is run for 48 h to reach a quasi steady state. The simulations are then continued from the startup simulation for another 24 h, which are used for the analysis presented here. The input parameters are averaged over a length of 131 days centering on 21 September 2004, which are as follows: IMF $B_x = 0.20$ nT, IMF $B_y = 0.13$ nT, IMF $B_z = -0.26$ nT, solar wind velocity, $V_x = 452$ km/s, $F_{10.7} = 99.2$ w/m$^2$/Hz, and hemispheric power, HP = 26.5 GW. The tides at the low boundary are turned off.

The CHAMP data set are used for comparison with GITM. CHAMP had a near-circular orbit at an inclination of 83.7°. The initial altitude was ~450 km [*Reigber et al.*, 2002], and during 2004 and 2005 the altitude decreased to ~380 km on average. The orbit covered all local times within 130 days, combining the ascending and descending nodes. The Planar Langmuir Probe (PLP) on board CHAMP measured the electron density every 15 s. A length of 131 days centered on September Equinox from 2004 to 2005 were analyzed in order to cover the full cycle of local times.

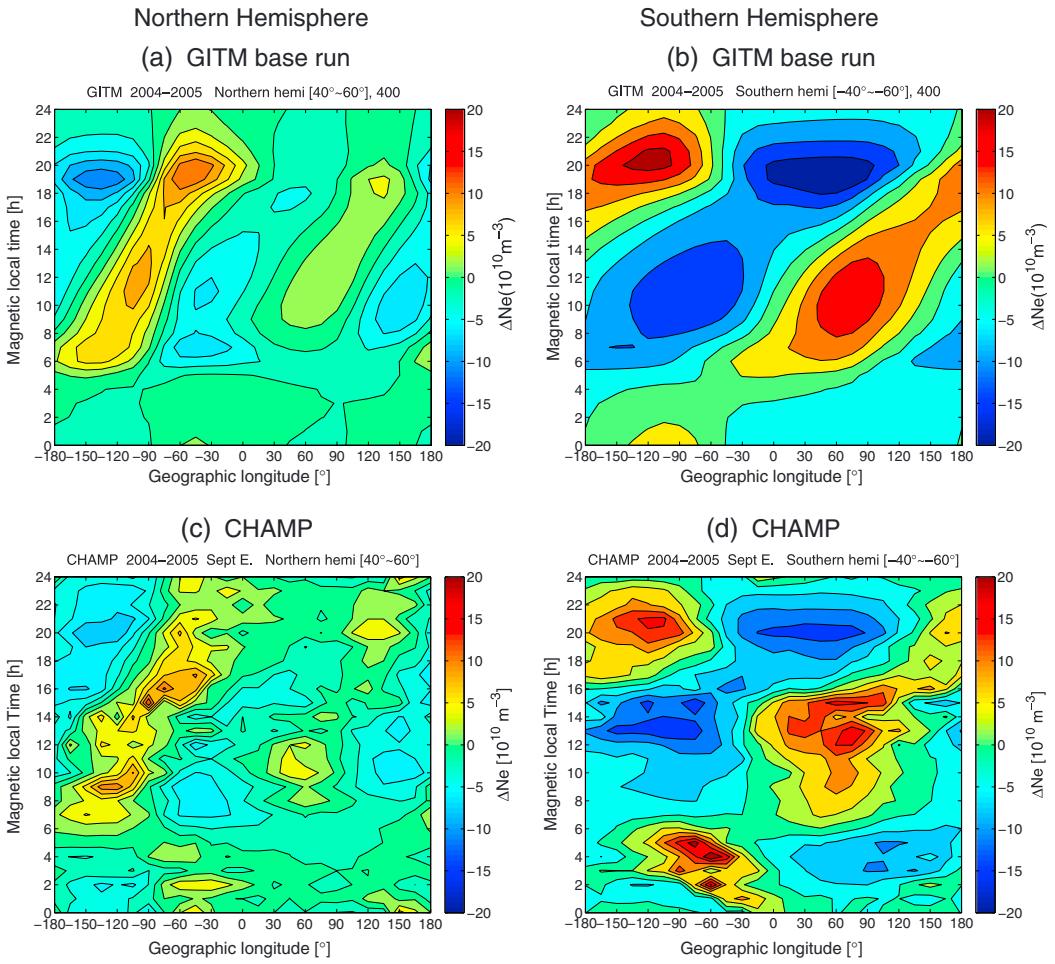


**Figure 1.** Geographical longitudinal versus magnetic local time variations of the difference in the electron density ($\Delta Ne$) simulated by (top row) GITM and observed by (bottom row) CHAMP in September in the (left column) Northern and (right column) Southern Hemispheres. Tides have been turned off at the lower boundary of the GITM model, and IGRF geomagnetic field model is used. Densities are given in $10^{10}$ m$^{-3}$.

## 3. Simulation Results

### 3.1. Comparison With CHAMP Observations

As a validation, GITM output is compared with CHAMP satellite observations. The midlatitudes between ±40° and ±60° magnetic latitudes (MLat) are considered. The electron density is sorted into geographic longitude (GLon) and magnetic local time (MLT) bins with a resolution of 15° longitude by 1 h MLT.

Figure 1 depicts contours of $\Delta Ne$ simulated by GITM at 400 km altitude (top row) and observed by CHAMP (bottom row) in both hemispheres in the frame of geographic longitude versus magnetic local time. The longitudinal mean value is subtracted for each MLT sector to show the longitudinal difference, $\Delta Ne$, which is dependent on MLT. Good agreement between the simulation results and observations exist in large-scale structures, with prominent wave-2 and wave-1 structure in the longitudinal profile in the Northern and Southern Hemispheres. Fine-scale structure is not presented in the model, since the results are for one single day driven by a 131 day average instead of a 131 day buildup of results, as is shown in the CHAMP results. The longitudinal differences reverse over the course of a day. The $\Delta Ne$ in the western America or western Europe-Asia appear during the daytime as a *Ne* enhancement and during the night as a *Ne* depletion. This reversal in $\Delta Ne$ is also seen in the Southern Hemisphere, i.e., higher *Ne* build up over Atlantic and Indian Oceans during the daytime, while over the Pacific Ocean areas, the $\Delta Ne$ increases at night. *Ne* perturbations are larger in the Southern Hemisphere than in the Northern Hemisphere, and larger in the Western Hemisphere (North America) than in the Eastern Hemisphere (Europe and Asia). The good

**Table 1.** Peak West-East Differences of *Ne* for Both Day and Nighttime Over Three Regions: North America, Europe-Asia, and Southern Ocean[a]

| Day (Nighttime) | Base Run | $U_z$ Effect | $U_m$ Effect | NW Effect | GSWM Tides |
|---|---|---|---|---|---|
| North America | 15.9 (23.6) | 15.7 (16.8) | −7.1 (−8.7) | 9.6 (8.6) | 3.1 (2.7) |
| Europe-Asia | 10.0 (9.8) | 8.2 (7.5) | - | 10.5 (8.0) | - |
| Southern Ocean | 33.2 (41.5) | 25.6 (31.5) | −16.2 (−12.6) | 23.7 (23.4) | - |

[a]From left to right are simulation results from the base run, zonal wind effect ($U_z$), meridional wind effect ($U_m$), neutral wind effect, and GSWM tidal effect. The values in the brackets are at nighttime. Reversed longitudinal differences from the normal pattern are shown as negative values. Areas without well-developed longitudinal pattern are not listed. Densities are given in $10^{10}$ m$^{-3}$.

agreement between the model and the observations give confidence that GITM is a suitable tool for investigating the mechanisms that account for the longitudinal differences of *Ne*. The peak west-east differences of Δ*Ne* over three sections, i.e., North America (180°W–0°W), Europe-Asia (0°E–180°E), and Southern Ocean areas (180°W–180°E), are determined for both the day and nighttime. These peak differences are listed in Table 1 and referred to as the base run. These quantities were used for comparison with the tests described below.

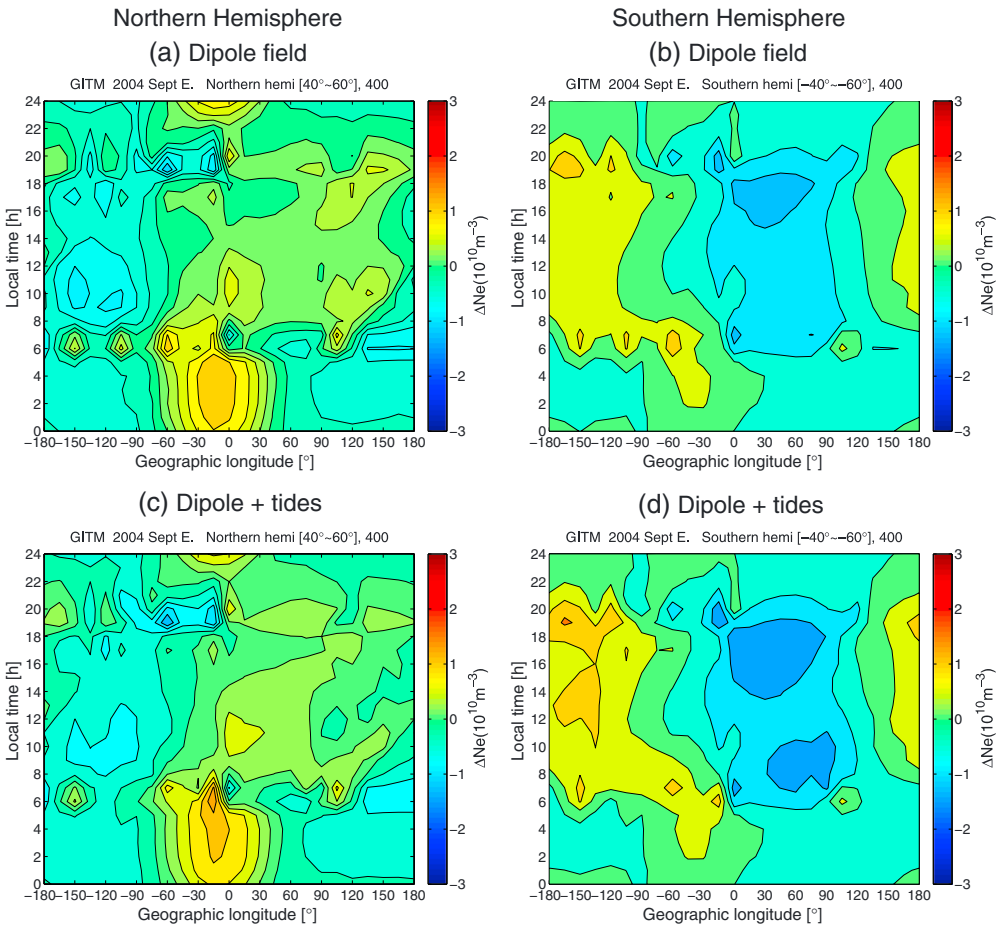


**Figure 2.** Geographical longitudinal versus magnetic local time variations of the difference in the electron density (Δ*Ne*) as simulated by GITM using the centered dipole magnetic field model. (a and b) Cases without tides. (c and d) Cases with GSWM migrating tidal forces imposed at the lower boundary of GITM. Densities are given in $10^{10}$ m$^{-3}$.

Eight test runs are performed using GITM model. Two tests are carried out using Earth-centered dipole magnetic field, with the dipole axis aligned with the rotation axis, one with no tides input from the lower atmosphere and the other with GSWM diurnal and semidiurnal migrating tides imposed at the low boundary of GITM. The other six tests are run in the presence of the actual IGRF field. Three of these runs test the neutral wind effects: zonal wind off, meridional wind off, and neutral wind off; here "off" means the vertical plasma drift due to the neutral wind is excluded in the simulation. One run tests the tidal effect: GSWM migrating tides are imposed at the low boundary of GITM. Two runs test whether the high-latitude activity has an effect on the electron density perturbations: the IMF $B_z$ is enhanced by a factor of 20, one run is with the neutral wind effect off, and the other run is with the neutral wind effect on. Through comparisons with the base run, the effects from the geomagnetic field, neutral wind, migrating tides, and high-latitude effect in the longitudinal configuration of *Ne* can be determined.

### 3.2. Geomagnetic Field Geometry

The simulation results of $\Delta Ne$ for runs with the centered dipole field are shown in Figure 2 in the same format as Figure 1. Figures 2a and 2c show the Northern Hemisphere, and the Figures 2b and 2d show the Southern Hemisphere. Figures 2a and 2b are simulations without tidal inputs from the lower atmosphere, and Figures 2c and 2d are with tidal inputs. Interestingly, the longitudinal differences in $\Delta Ne$ disappear in both hemispheres irrespective of the tidal input. This indicates that the geometry of the geomagnetic field is vital in making the longitudinal difference of *Ne*. The migrating tides at the lower boundary of GITM have almost no effect on the zonal modulation of the *F* region ionosphere at midlatitudes.

### 3.3. Neutral Wind Effect

Three runs are shown in Figure 3 to illustrate the neutral wind effect. Figures 3a–3f are runs that demonstrate the effect of the meridional wind, zonal wind, and neither on the vertical plasma velocity. When the zonal wind effect is removed (Figures 3a and 3b) and only the meridional wind is considered, the $\Delta Ne$ patterns are very different from the base results shown in Figure 1. The daytime *Ne* disturbances shift eastward by about 30°. Over North America (180°W–0°W), reversed west-east difference as compared to the observations and the base case can be found, with larger daytime *Ne* occurring to the east. The nighttime zonal difference remains similar in shape as the base case, but is significantly reduced.

In order to isolate the effect that the zonal wind has on the system, the simulation that excludes the zonal wind (i.e. meridional wind included only) is subtracted from the base simulation. The difference should then be the contribution exclusively from the zonal wind. Density differences between runs with and without zonal wind effects ($Ne_{\text{rest}} = \Delta Ne_{\text{base}} - \Delta Ne_{U\text{off}}$) are shown in Figures 4a and 4b. There are two zones of enhancements and two zones of reductions of *Ne* along a local time profile in the Northern Hemisphere and one zone of enhancement and one zone of reduction in the Southern Hemisphere. The prenoon peaks (troughs) are in nearly the same longitude as the afternoon troughs (peaks). This opposite phase in *Ne* disturbances over the same geographic area is the manifestation of opposite effects of the prenoon westward and afternoon eastward zonal winds. The longitudinal difference is larger in the Western-Northern Hemisphere than in the Eastern Hemisphere, and larger in the Southern Hemisphere than in the Northern Hemisphere. The peak longitudinal differences over North America, Europe-Asia, and Southern Ocean areas are listed in Table 1. Compared to the base run, the longitudinal differences caused by the zonal wind amount to 80% of the original differences, on average. Here the percentage is the averaged value with all peaks for runs with zonal wind effects divided by those for base run as listed in Table 1.

When the meridional wind effect is off, as shown in Figures 3c and 3d, the longitudinal difference of $\Delta Ne$ gets enhanced in amplitude. The meridional wind effect is more clearly presented with residual values ($Ne_{\text{rest}} = \Delta Ne_{\text{base}} - \Delta Ne_{U\text{moff}}$, $U_m$ is the meridional wind), as shown in Figures 4c and 4d, one can find opposite west-east difference of *Ne* in the MLT sectors of 6–24 h over North America (180°W–0°W) and Southern Ocean areas (180°W–180°E). The longitudinal pattern over the European-Asian sector (0°E–180°E) is not well developed. Interestingly, the equatorward wind is effective over the Pacific ocean (180°W–30°W) in the early morning, which raises the $\Delta Ne$ level.

The simulated *Ne* with no neutral wind contributions is shown in Figures 3e and 3f. Similar longitudinal and diurnal patterns exist as in the observations, but they are reduced in magnitude both during the day and nighttime. In particular, over the European and Asian sector (0°E–180°E) and in the nighttime of South Pacific Ocean (180°W–30°W), the electron densities become rather weak. Further illustrated in Figures 4e and 4f are differences between runs with and without neutral wind effects, which represent the total effect

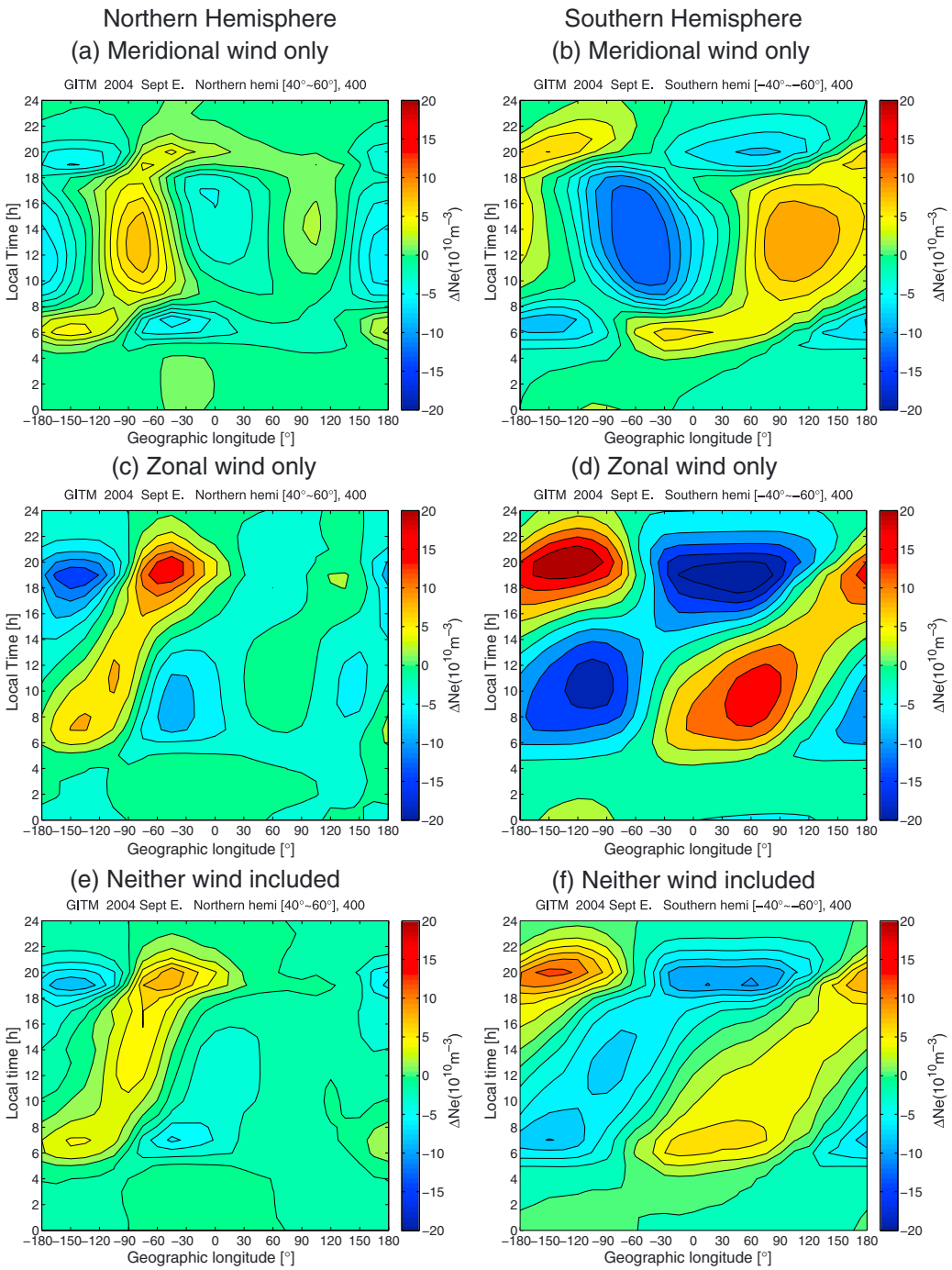


**Figure 3.** Geographical longitudinal versus magnetic local time variations of the difference in *Ne* as simulated by GITM in the presence of IGRF field. Cases have included the effects from the (a, b) meridional winds (i.e., zonal winds excluded), (c, d) zonal winds (i.e., meridional winds excluded), and (e, f) neither.

that the neutral winds have on the longitudinal asymmetries in electron density. The longitudinal differences caused by the neutral winds are larger in the south than in the north but quite comparable over European-Asian versus North American areas, in which the effects from the zonal and meridional winds are out of phase. The *Ne* in the early morning in the South Pacific Ocean region maintained a high level due to the positive contributions from both the zonal and meridional winds. The neutral winds contributed on average 68% to the observed longitudinal difference (see Table 1).

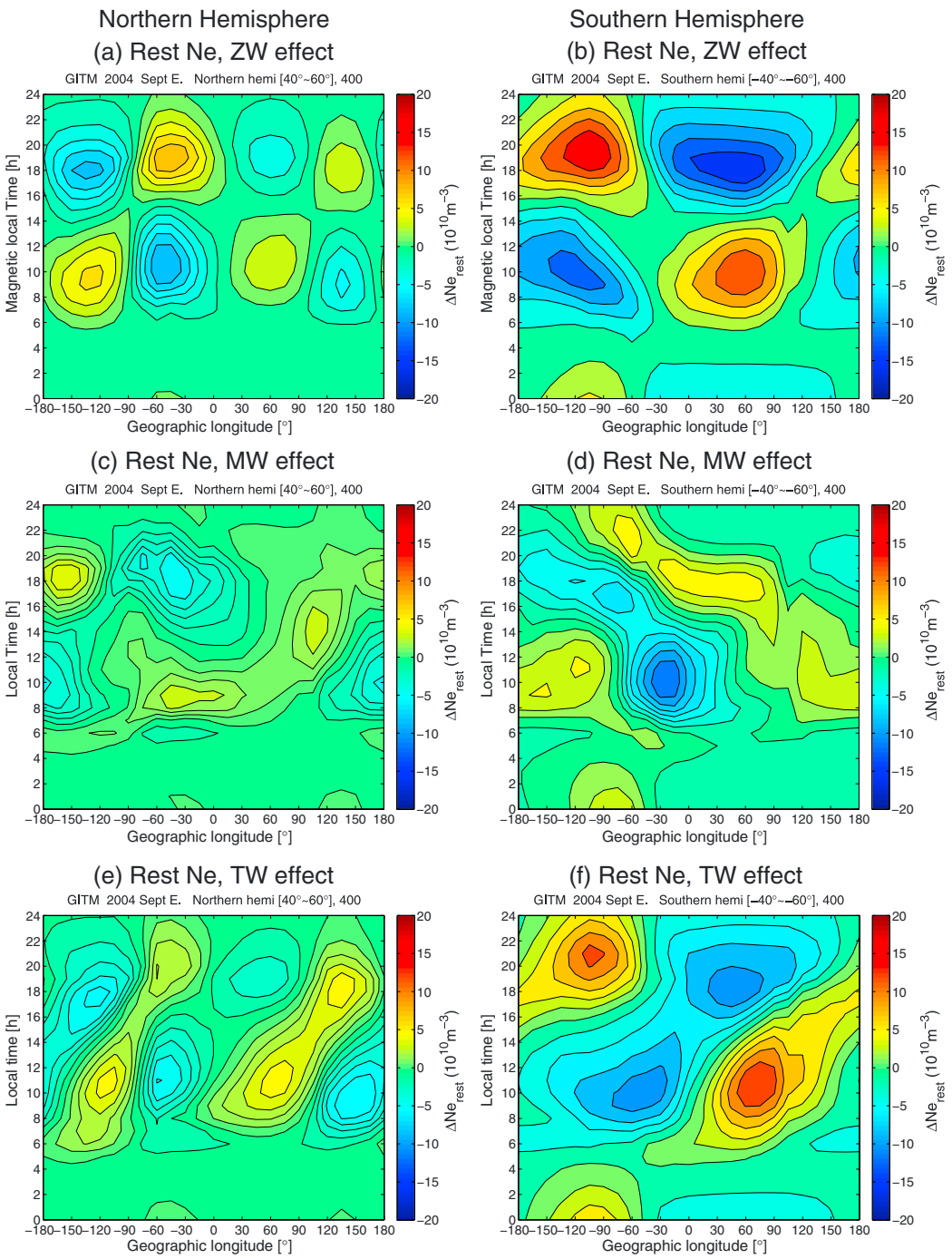


**Figure 4.** The same as in Figure 3 but for $Ne_{rest}$, which means the residual value of *Ne* after the subtraction of runs shown in Figure 3 from the base run. Therefore, $Ne_{rest}$ represents effects from the (a, b) zonal wind, (c, d) meridional wind, and (e, f) total wind, respectively.

### 3.4. Tidal Effect

Another simulation was conducted to check whether migrating tides from the lower atmosphere in the presence of actual magnetic field (IGRF) could have an effect on the longitudinal distribution of the electron density at midlatitudes. As shown in Figure 5, when GSWM diurnal and semidiurnal migrating tides are set as the low boundary of GITM, the longitudinal and diurnal patterns remain almost unchanged as compared to the base run. The amplitude of $\Delta Ne$ is enhanced by about 15% over North America (180°W–0°W).

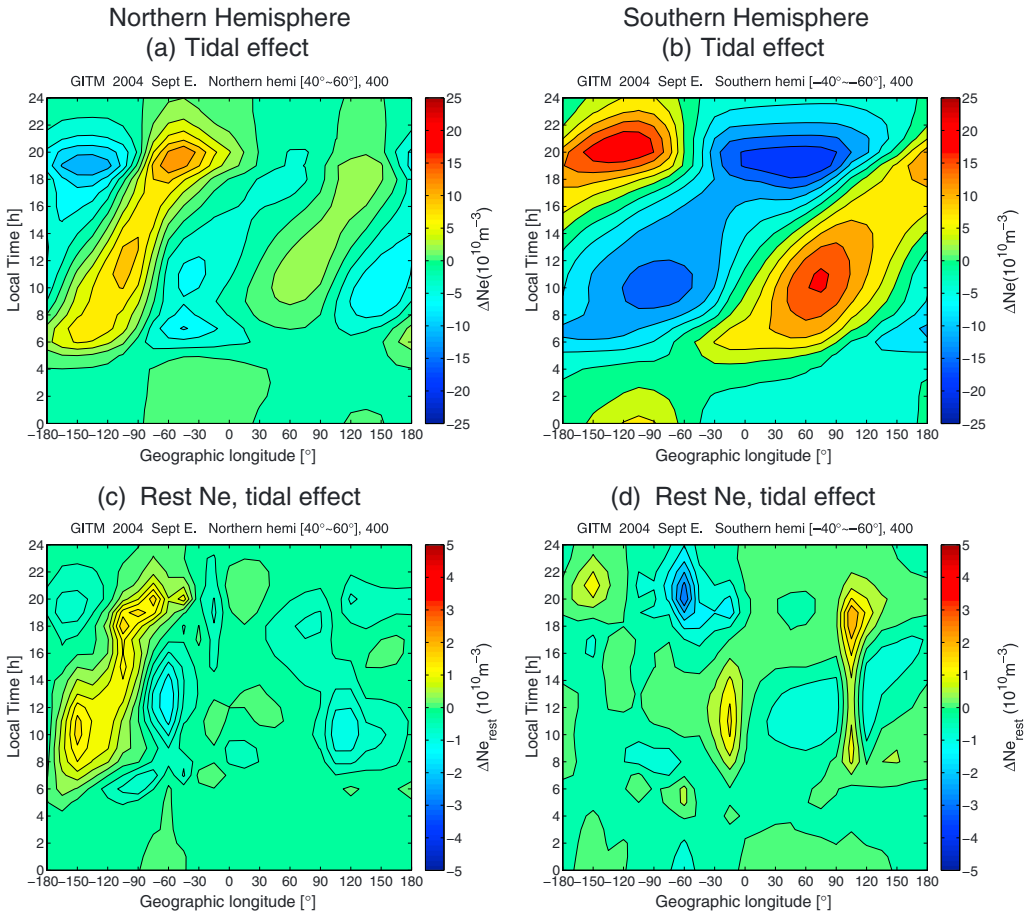


**Figure 5.** Same format as Figure 1 but for the case when diurnal and semidiurnal migrating tides are imposed at the low boundary of GITM. (a and b) Geographical longitudinal versus magnetic local time variations of the difference in *Ne*. (c and d) Residual *Ne* after the subtraction of the previous base run.

The migrating tides have no impact on the midlatitudinal longitudinal pattern of *Ne* over the European-Asian (0°E–180°E) and Southern Ocean areas (180°W–180°E).

### 3.5. High-Latitude Effect

Strong horizontal wind can be generated in the auroral region during periods of strong magnetic activity. These winds can carry molecular-rich air from high latitudes to midlatitudes and cause both composition and wind disturbances there [e.g., *Proelss*, 1981; *Fuller-Rowell et al.*, 1994]. The equatorward wind adds to (reduces) the nighttime (daytime) background equatorward (poleward) wind. Furthermore, the equatorward wind turns westward due to the Coriolis force, which can weaken (strengthen) the nighttime (daytime) eastward (westward) zonal wind. The molecular-rich air can increase the chemical recombination rate at midlatitudes, which results in the decrease in *Ne*. In order to check the effect of high-latitude activity on the midlatitudinal electron density structuring through the composition changes due to increased winds, IMF $B_z$ was enhanced by a factor of 20. The interplanetary electric field was correspondingly changed from 0.12 mV/m to 2.4 mV/m ($E_y = V_x \times B_z$), which resulted in enhancements of the high-latitude electric field and Joule heating. The neutral wind effects on the vertical plasma motion were turned off in order to isolate the effect of the composition changes.

As seen in Figure 6, Δ*Ne* exhibits a different longitudinal and diurnal distribution than the normal pattern as depicted in Figures 3e and 3f. Daytime wave-2 structures emerge in both hemispheres, which do not reverse in local time. The residual *Ne*, after a subtraction of the baseline distribution, is shown in Figures 6c and 6d. The main differences between these two runs exist in the daytime from 6 to 22 MLT. There are wave-2 structures along the longitudinal profile in both hemispheres. In the Northern Hemisphere, there are two zones with enhanced density near 90°W and 90°E and two zones of depleted density centered around 30°W and

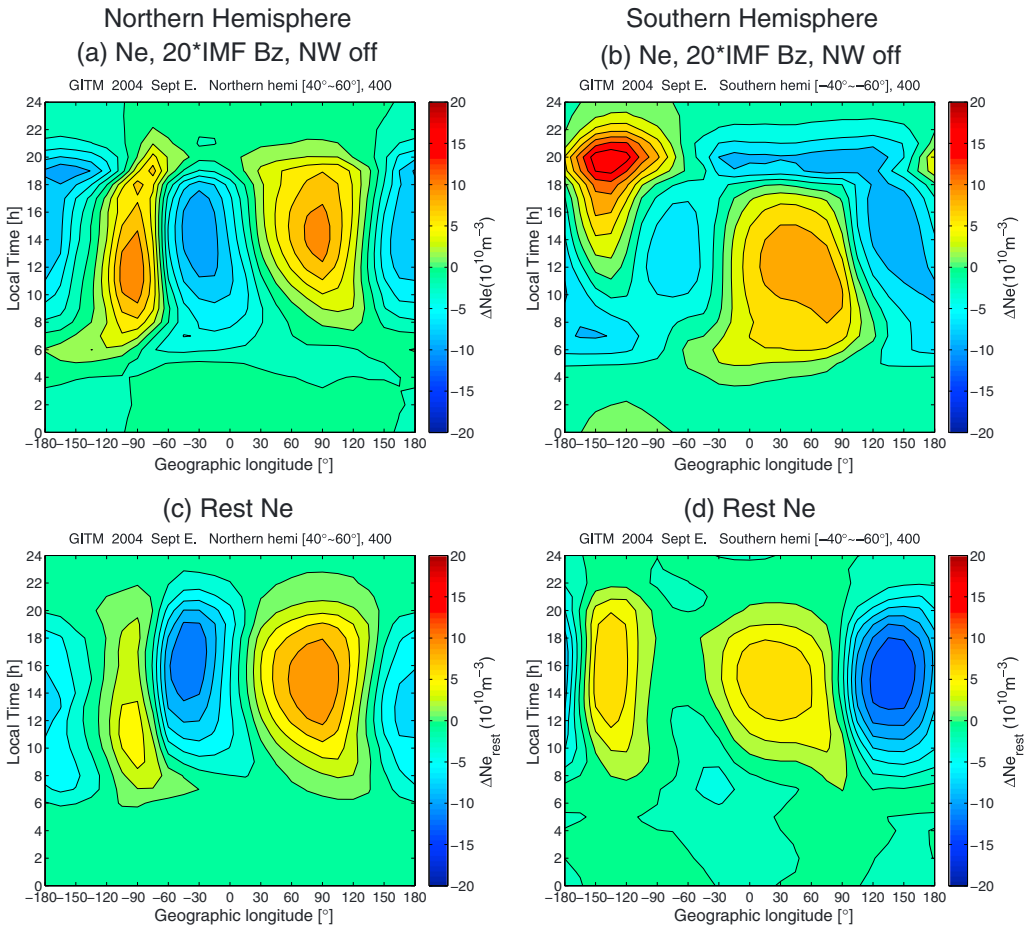


**Figure 6.** Same format as Figure 3 but for the case when IMF $B_z$ is enhanced by a factor of 20. The total wind effect is excluded for the present run to isolate the thermospheric composition effect. (a and b) Geographical longitudinal versus magnetic local time variations of the difference in *Ne*. (c and d) are residual *Ne* after the subtraction of the run with the total wind off (Figures 3e and 3f) from the present case.

180°E longitude. In the Southern Hemisphere, the depletions and enhancements are shifted between 30° and 60° from the Northern Hemisphere.

## 4. Discussion

Based on the agreement between the GITM simulation and CHAMP observations at different local times and longitudinal sectors, the model is employed to study the relative contributions of various physical processes to the longitudinal structuring of the electron density. In particular, the present work focuses on effects of the magnetic field geometry, horizontal neutral winds, migrating tides from the lower atmosphere, and high-latitude activity.

### 4.1. Geomagnetic Field Geometry

The longitudinal variation of the electron density is strongly dependent on the displacement of the geomagnetic from the geographical pole, which causes a zonal asymmetry of the magnetic declination angle at midlatitudes. This is supported by the fact that the longitudinal difference of *Ne* vanishes when the geomagnetic axis was aligned with the geographic rotation axis (see Figure 2). For the case with the aligned dipole magnetic field, the geographic and geomagnetic coordinate systems overlap with each other. The magnetic declination angle becomes zero, and the local time dependence of the neutral wind becomes independent of longitude. Thus, in the simulation results using an aligned dipole, there is no contribution of the neutral wind to the longitudinal dependence of *Ne*, which explains the disappearance of the longitudinal variation of *Ne*, for the most part (this will be discussed in more detail below). The actual north magnetic pole is approximately 10° displaced from the geographic pole, while the south magnetic pole is displaced by over

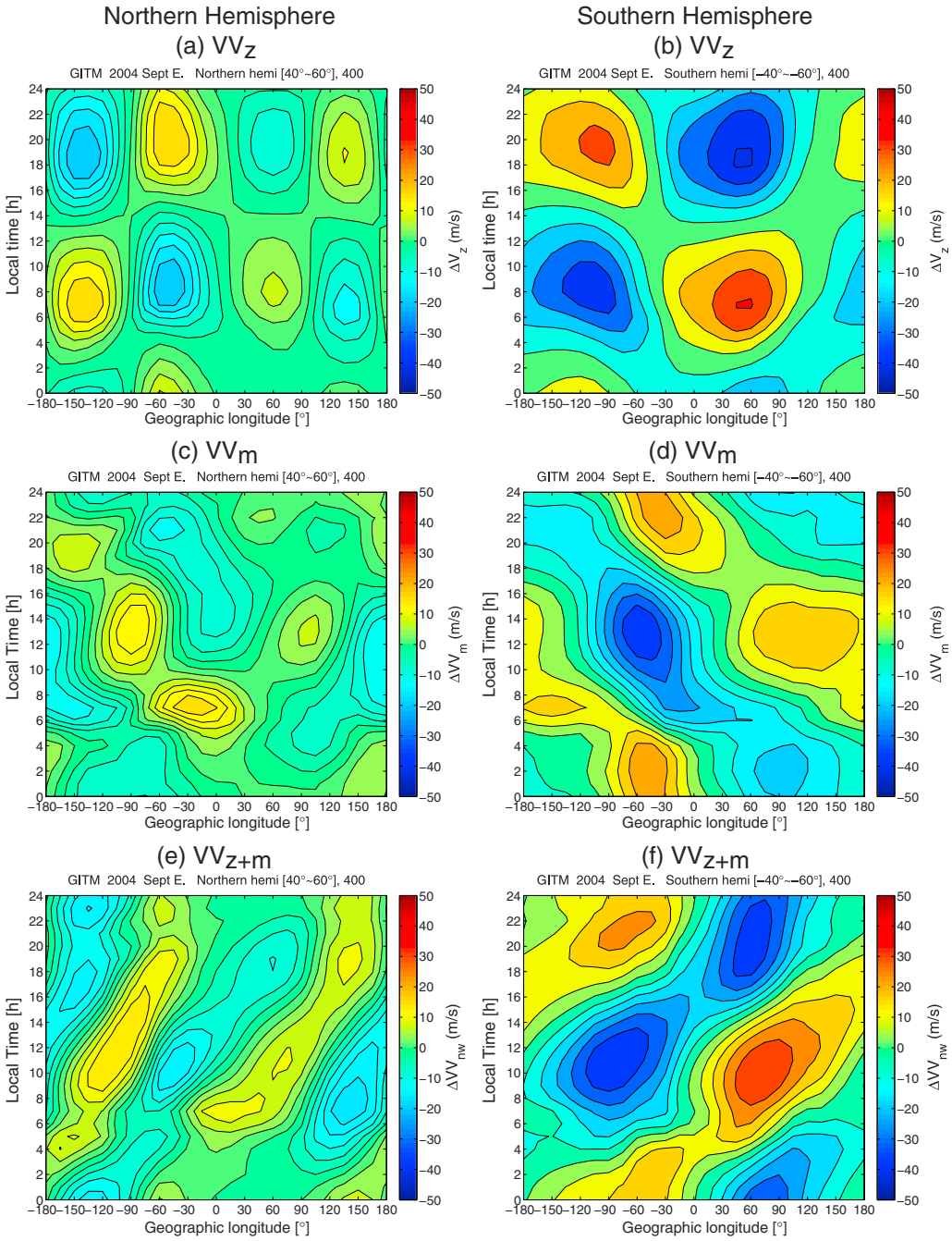


**Figure 7.** Geographical longitudinal versus magnetic local time variations of the difference in the vertical plasma flow due to the (a, b) zonal wind ($\Delta VV_z$), (c, d) meridional wind ($\Delta VV_m$), and (e, f) total wind ($\Delta VV_{z+m}$) as simulated by GITM for the base case as shown in Figures 1a and 1b. Velocities are given in meters per second.

15°. In the Southern Hemisphere there are larger declination angles at midlatitudes than in the northern midlatitudes. Subsequently, the longitudinal difference of *Ne* is more prominent in the south than in the north, which is shown in both the simulation and the observation (see Figure 1).

### 4.2. Neutral Wind Effect

Due to the nonzero geomagnetic declination and inclination angles, the neutral winds can contribute to the vertical motion of the plasma. This vertical velocity (*VV*) can be expressed as follows:

$$VV = U_m \cos D \cos |I| \sin |I| \mp U_z \sin D \cos |I| \sin |I|, \quad (1)$$

where the negative and positive signs correspond to the Northern and Southern Hemispheres, respectively. $U_m$ and $U_z$ are the geographic meridional and zonal wind (positive for equatorward and eastward wind), $D$ is magnetic declination (positive for eastward), and $I$ is magnetic inclination angle (positive in the north and negative in the south). $D$ and $I$ are calculated from the International Geomagnetic Reference Field (IGRF) model [*Maus et al.*, 2005]. When the resultant vertical velocity is positive, the plasma will be pushed up the magnetic field to regions of less molecular neutral species, reducing the loss of the $O^+$, such that the electron density will increase during the day. If the vertical velocity is negative, the reverse will occur.

Figure 7 shows the vertical plasma velocity due to the zonal wind ($\Delta VV_z$), meridional wind ($\Delta VV_m$), and total neutral wind effect ($\Delta VV_{m+z}$) for the base run (Figure 1). The impact of the zonal wind on the vertical plasma flow depends on the sign of the geomagnetic declination angle (i.e., sin $D$). There are two positive (eastward) and negative (westward) declination zones in the Northern Hemisphere, while there is one positive and negative zone in the Southern Hemisphere. Therefore, the longitudinal variation induced in the electron density by the declination angle are two (one) enhancement zones and two (one) reduction zones for a constant local time in the Northern (Southern) Hemisphere. These explain the wave-2 and wave-1 structures in $\Delta VV_z$ shown in Figure 7 (i.e., two peaks and two valleys in the Northern Hemisphere and one peak and one valley in the south). The variation at a constant longitude is affected by the diurnal changing of the zonal wind. The zonal wind is westward in the prenoon sector and eastward in the postnoon sector, thus making the longitudinal difference reverse near noon. The longitudinal and diurnal pattern of $VV_z$ is similar to that of $\Delta Ne$ as shown in Figures 4a and 4b, thus supporting the zonal wind mechanism established by other researchers [e.g., *Zhang et al.*, 2011]. In both hemispheres, there was about a 2–3 h delay between the plasma density variations and the vertical plasma motion in the prenoon sector. This implies that in the morning sector the vertical motion of ions takes an hour or two to affect the electron density, while in the afternoon sector, the electron density is affected immediately by the vertical motion.

The longitudinal and diurnal variations in the vertical plasma velocity due to the meridional wind are unaffected by the sign of the declination angle (i.e., cos $D$). These variations are more related to the longitudinal and diurnal variation of the meridional wind, because the magnetic inclination angle term (i.e., sin $I$·cos $I$) has smaller longitudinal variation in the magnetic midlatitudes (40°–60° MLat) as compared to the meridional wind (the longitudinal pattern of the meridional wind is quite similar to the vertical velocity, figure not shown). In the Northern Hemisphere, wave-1 (wave-2) structure along the longitude can be found before (after) noon. In the Southern Hemisphere, wave-1 structure exists in the longitudinal profile. In comparison with Figures 4c and 4d, the longitudinal and diurnal distribution of the meridional wind and $\Delta Ne$ are very similar.

In Figures 7e and 7f are shown the vertical velocity due to the total neutral wind. The up-lifting or down-pushing effect from the zonal and meridional winds can be opposite to each other, for example, over North American sector. The maximum uplift effect from the zonal and meridional winds can be separated by tens of degrees, for example, in the early morning of South Pacific Ocean. Subsequently, the maximum up-lifting occurs in between them. The longitudinal and local time patterns of the vertical plasma velocity resulting from the total wind resembles the patterns of $\Delta Ne$ as shown in Figures 4e and 4f. The neutral wind effect provides vertical momentum to the plasma, pushing them up or down, thus playing a critical role in forming the longitudinal distribution of $Ne$.

In summary, the zonal wind can account for approximately 80% the observed west-east difference in $Ne$. The meridional winds reduce the effect of the zonal wind to 68% in the North American and Southern Ocean areas, since meridional winds have roughly the opposite effect as the zonal wind. The longitudinal positions of $Ne$ peaks and troughs caused by the zonal winds are shifted by the meridional winds. Both zonal and meridional winds contribute positively to the development of the longitudinal difference in the premidnight sector of the South Pacific Ocean (180°W–30°W).

### 4.3. Tidal Effect

Migrating tides from the lower atmosphere do not drive the zonal difference of $Ne$ in the presence of an aligned dipole field, as shown in Figures 2c and 2d. But in the presence of the actual magnetic field, migrating tides do contribute to the longitudinal difference of $Ne$ by about 15%, primarily in the North American area. Previous studies have shown that the nonlinear interaction between migrating tides and the geomagnetic field configuration can generate nonmigrating tides [e.g., *Hagan and Roble*, 2001; *Wu et al.*, 2012a]. For example, DW1 (migrating tide) and SPW1 (Stationary planetary waves) can generate D0

and DW2 (nonmigrating tides). The nonmigrating tides can cause longitudinal and local time dependencies in the electron density [e.g., *Xiong and Lühr*, 2014; H. Wang et al., submitted manuscript, 2015]. However, the midlatitude model results presented here suggest that the migrating tides at midlatitudes decayed significantly before being coupled with the upper thermosphere and ionosphere. Previous work have shown that nonmigrating tides originate in the troposphere can modulate the longitudinal pattern of ionosphere and thermosphere at equatorial regions [e.g., *Hagan and Forbes*, 2002; *Immel et al.*, 2006; *Wu et al.*, 2008, 2009; *Wan et al.*, 2010; *Lühr et al.*, 2012; *Wu et al.*, 2012b; *Chang et al.*, 2013]. The detailed investigation of the nonmigrating tides effects on the midlatitudinal longitudinal pattern of *Ne* will be left for future work.

### 4.4. Solar Illumination

As discussed above, about 68% of the longitudinal variation of the electron density is accounted for by the neutral winds, and approximately 15% may be accounted for by the tides, leaving roughly 17% or so unaccounted for. One has to ask the following question: what kind of physical process can drive the remaining contribution to the longitudinal pattern in the electron density (see Figures 3e and 3f)? Since the primary source of the ionosphere is the solar EUV/UV radiation, it might be interesting to check the longitudinal dependence of the solar illumination.

The longitudinal and diurnal variations of ΔSZA (solar zenith angle, SZA) are shown in Figure 8. Figures 8a and 8b are for the aligned dipole magnetic field, and Figures 8c and 8d are for the IGRF field (base run). Positive value means increased SZA (i.e., less sunlight) from the longitudinal mean. Roughly speaking, SZA $<100°$ is in sunlight, while SZA $\geq 100°$ is in darkness at 400 altitudes [*Wang et al.*, 2005]. The overlayed white line indicates this demarkation (i.e., SZA $= 100°$), which separates the illuminated dayside and the dark nightside.

For the centered dipole field case, since the geomagnetic and geographic poles are aligned with each other, the solar illumination is independent of longitude. However, within the IGRF frame, longitudinal variations of the solar illumination exist (as shown in Figures 8c and 8d), due to the fact that the magnetic midlatitudes occur at different geographic latitudes depending on the longitude. The ΔSZA shows a wave-1 structure along the longitude profile in both hemispheres. The daytime solar illumination is perturbed the most around 90°W GLon in the Northern Hemisphere, while there are two areas of strong perturbation in the Southern Hemisphere: around 90°W and 120°E. These two sectors (90°W and 120°E) are in the vicinity of the north and south magnetic poles. Figures 8e and 8f show the longitudinal and magnetic local time variation of the averaged geographical latitudes in the magnetic latitude bands from ±40 to ±60°). As illuminated in Figures 8e and 8f, in the Northern Hemisphere the geographic latitude of the middle magnetic latitude is 39° at 90°W (near pole), while it is 56° at 120°E (far from pole). In the Southern Hemisphere the geographical latitude of the middle magnetic latitude is 37° in the near-pole sector (120°E), while it is 64° in the far-from-pole sectors (90°W). The difference in the geographical latitude is the key point for the zonal dependence of the SZA.

No obvious longitudinal differences of SZA exist over European-Asian sector because of less longitudinal variation of the geographical latitude. The solar illumination effect in the Southern Hemisphere is larger than in the Northern Hemisphere. Subsequently, the longitudinal dependence of the electron density is larger in the south than in the north (see Figures 3e and 3f). The largest perturbations are observed at sunrise and sunset, with almost no perturbations occurring at night and weak perturbations during midday. This points strongly to the solar zenith angle effect. Comparing Figures 3e and 8c as well as Figures 3f and 8d, similarities exist. For example, in the Northern Hemisphere, the largest perturbations occur near 120°W in both the SZA and Δ*Ne*, while in the Southern Hemisphere, all longitudes are affected by both the SZA and the Δ*Ne*. The Δ*Ne* is larger in the Southern Hemisphere, while the SZA effect is more prominent there, too. Therefore, it is argued that the majority of the nonneutral-wind-driven Δ*Ne* may be caused by the longitudinal dependence of the SZA in magnetic coordinates.

### 4.5. High-Latitude Effect

When the southward IMF $B_z$ is enhanced significantly, more energy is deposited into the high-latitude ionosphere. Enhanced Joule heating in the auroral zone will cause stronger equatorward neutral winds, which can transport $N_2$-molecular-rich air from the high latitudes to midlatitudes, thus increasing the charge exchange and subsequently the recombination rate in the region [e.g., *Seaton*, 1956; *Proelss*, 1980; *Fuller-Rowell et al.*, 1994; *Rishbeth*, 1998]. The neutral wind effect on the vertical motion of the plasma is turned off in this run, so that the wave-2 structure of the electron density in the longitudinal profile

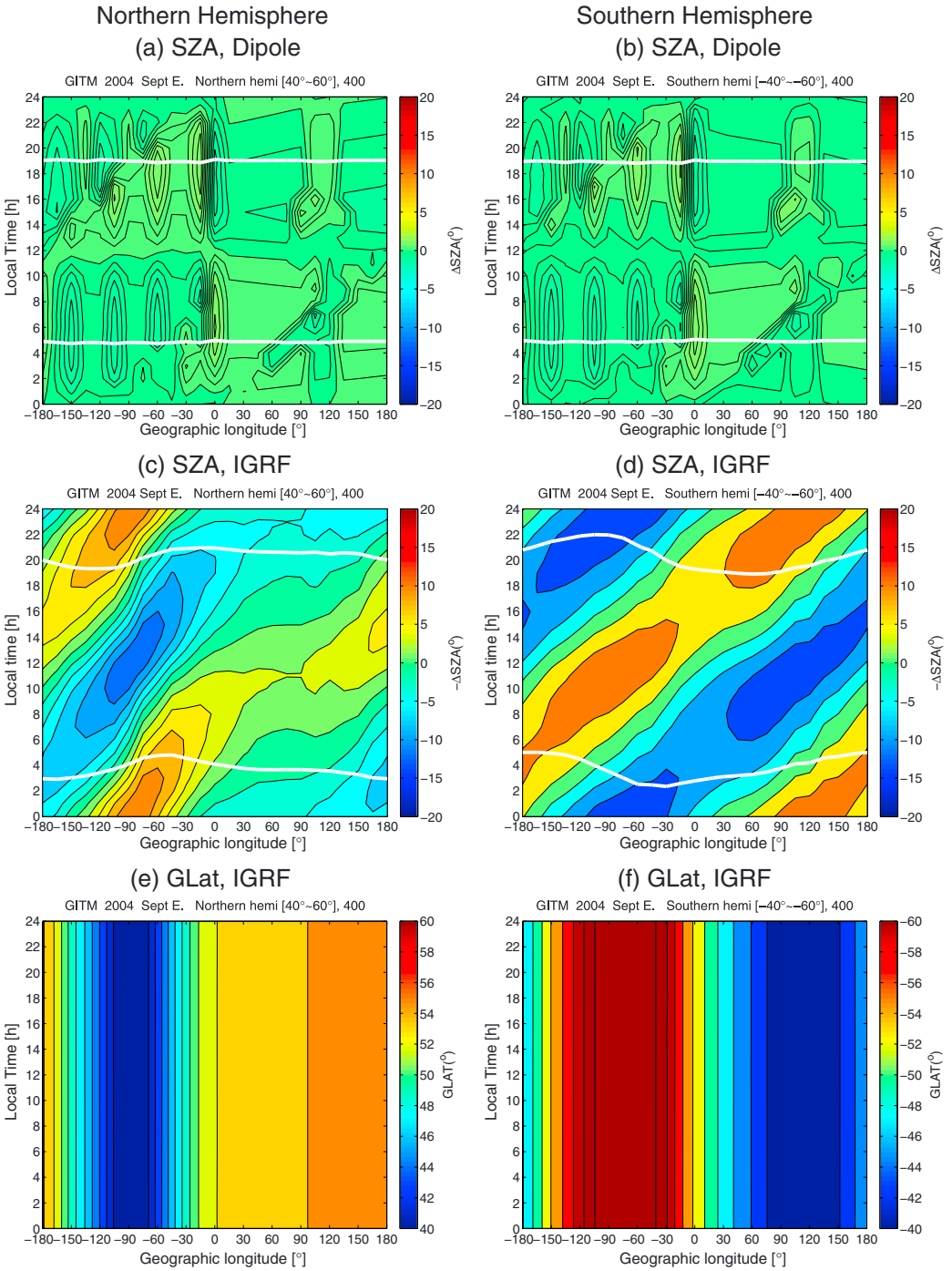


**Figure 8.** Geographical longitudinal versus magnetic local time variations of the difference in the solar zenith angle (ΔSZA). Overplotted white lines indicate the solar terminator position (SZA = 100°). (a and b) The centered dipole magnetic field case. (c and d) The IGRF magnetic field case. (e and f) Geographical latitudes at magnetic midlatitudes for the IGRF magnetic field case. Angles are given in degrees.

(see Figures 6c and 6d) originates primarily from the compositional changes within the thermosphere at midlatitudes, which are determined by the circulation. In the *F* region, the production of $O^+$ comes primarily from the photo-ionization of atomic oxygen (O), while the loss is mainly through charge exchange with the molecular nitrogen ($N_2$) and the subsequent rapid dissociative recombination of the $N_2^+$ [e.g., *Seaton*, 1956]. Thus, the composition ratio between atomic oxygen and molecular nitrogen ($O/N_2$) largely determines the electron density, and a decrease in $O/N_2$ could lead to a decrease in the electron density in the *F* region.

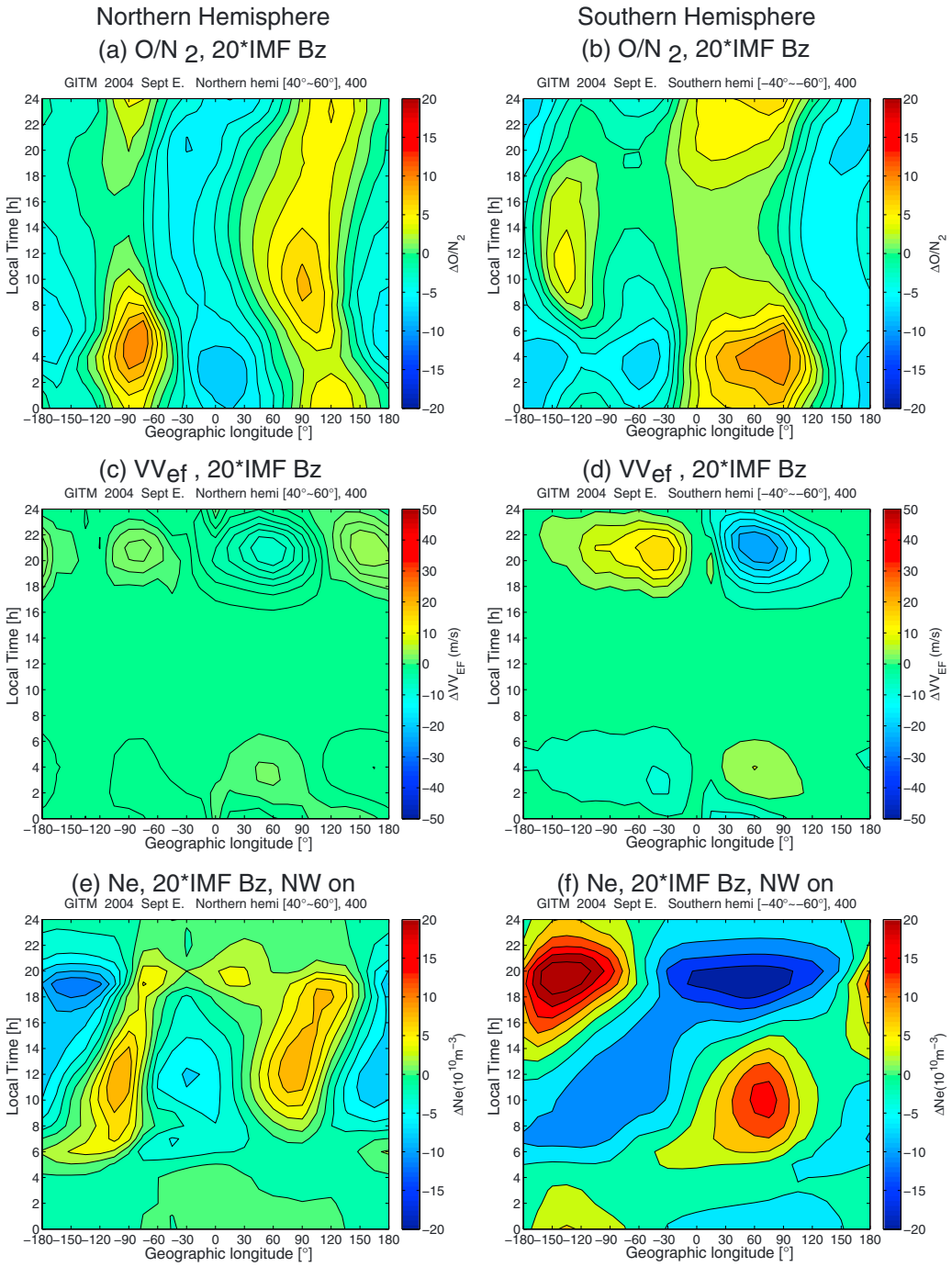


**Figure 9.** Geographical longitudinal versus magnetic local time variations of the (a and b) difference of the ratio between O and $N_2$ densities and $\Delta O/N_2$, and (c and d) the vertical plasma velocity due to the midlatitudinal electric field, $\Delta VV_{EF}$. Both parameters are for the enhanced IMF $B_z$ case as shown in Figure 6. (e and f) The longitudinal and diurnal variation of *Ne* for the case with enhanced electric field but with the neutral wind effects included.

Figures 9c and 9d show the longitude versus the local time variation of the composition ratio. There is a prominent wave-2 longitudinal variation (i.e., two-peak and two-trough in the longitude). The peaks maximize in the early morning sector, and the phases of the variation appear to have been almost stationary during the whole day. In the Northern Hemisphere, the $O/N_2$ ratio is larger in the longitudinal sector near 90°W and 120°E than in other longitudinal sectors. In the Southern Hemisphere the behavior is more complex but appears to be roughly 60° out of phase with the Northern Hemisphere variations. Observational

studies describing the tidal structure of $O/N_2$ in the midlatitudes are not available, so it is difficult to determine whether these are realistic patterns. However, previous studies have reported a wave-4 or wave-3 longitudinal structure within the $O/N_2$ ratio in the equatorial region, which shows similar longitudinal behavior as the electron density [e.g., *He et al.*, 2010; *Kil and Paxton*, 2011]. The longitudinal patterns of the $O/N_2$ are consistent with the electron density (see Figures 6c and 6d), showing the importance of the neutral composition in determining the longitudinal modulation of the electron density.

The midlatitudinal electric field ($\vec{E}$) can contribute to the vertical motion of plasma in the *F* region, due to the fact that the magnetic field at midlatitudes is inclined. This leads to a vertical component to the $\vec{E} \times \vec{B}$ drift. As illustrated in Figures 9c and 9d, the midlatitude electric field impacts the electron density primarily during the night, and the effect is more significant in the south than in the north. However, the electric field effect is smaller than the neutral composition change effect, as can be seen by comparing Figures 9c and 6c as well as Figures 9d and 6d.

For comparison, the longitudinal variations of *Ne* due to both the neutral wind and compositional changes are illustrated in Figures 9e and 9f. The effect of the composition change of the thermosphere is discernable in the Northern Hemisphere but is mostly absent in the Southern Hemisphere. In the Southern Hemisphere the neutral wind mechanism plays a dominant role, but the composition does affect the shape of the zonal variation of *Ne*. For example, *Ne* over the South Pacific Ocean (180°W–30°W) is enhanced in amplitude.

## 5. Summary

The global ionosphere-thermosphere model has been employed to explore the relative importance of various possible physical drivers of the longitudinal dependence within the electron density at midlatitudes. Nine simulations have been carried out to examine the impacts of the geomagnetic field geometry, zonal wind, meridional wind, migrating tide from the lower atmosphere, high-latitude activity, and solar illumination on the electron density in quantitative ways. The major findings based on the comprehensive simulations performed in the study are summarized as follows:

1. The geomagnetic field geometry (magnetic tilt away from the rotation axis and declination) is vital in the formation of the longitudinal dependence of *Ne*. The asymmetries in the magnetic field geometry results in both hemispheric and interhemispheric asymmetries of *Ne*.
2. The zonal wind contributes to about 80% of the fraction of the observed longitudinal dependence of *Ne*. The meridional wind reduces the wind contribution to the longitudinal dependence to 65% over North America and Southern Ocean areas. Both contribute to the higher density in the postmidnight sector of the South Pacific Ocean.
3. Migrating diurnal and semidiurnal tides from the lower atmosphere can increase the longitudinal difference of *Ne* by about 15% over North America within the actual magnetic field frame.
4. Solar ionization plays an important role in modulating the background pattern of *Ne*, due to the fact that the magnetic field is tilted so that the midlatitudes are at lower geographical latitudes in some longitudinal sectors and at higher geographic latitudes in other longitudinal sectors. The solar illumination most strongly affects the longitudinal distribution of *Ne* over North America and Southern Ocean areas.
5. Enhanced high-latitude activity alters the longitudinal distribution of *Ne*, through transporting molecular-rich air from the high latitudes to midlatitudes as well as altering the wind pattern. The $O/N_2$ density ratio exhibits wave-2 longitudinal variation.

**Acknowledgments**

The operational support of the CHAMP mission by the German Aerospace Center (DLR) and the financial support for the data processing by the Federal Ministry of Education (BMBF), as part of the Geo-technology Programme, are gratefully acknowledged. The authors thank GFZ ISDC for providing CHAMP electron data through http://isdc.gfz-potsdam.de (or contact Jan Rauberg, jan.rauberg@gfz-potsdam.de). The solar wind and IMF data are from NASA/GSFC's Space Physics Data Facility's OMNIWeb service (ftp://spdf.gsfc.nasa.gov/pub/data/omni/low_res_omni/). The National Oceanic and Atmospheric Administration (NOAA) provides the hemispheric power data at http://www.sec.noaa.gov/ftpdir/lists/hpi. The solar radio flux $F_{10.7}$ data can be found at ftp://ftp.ngdc.noaa.gov/STP/SOLAR_DATA/SOLAR_RADIO/FLUX. GITM model was developed by the University of Michigan (contact Aaron Ridley, ridley@umich.edu). This work is supported by the National Nature Science Foundation of China (41222030, 41221003, and 41431073), Program for Young Top Talents by the Organization Department of China, Program for New Century Excellent Talents in University by the Ministry of Education, and the Specialized Research Fund for State Key Laboratories. Research is also supported by award ATM1138938 from the National Science Foundation.

Alan Rodger thanks Gopi Seemala and another reviewer for their assistance in evaluating this paper.

## References

Bilitza, D. (2001), International Reference Ionosphere 2000, *Radio Sci.*, *36*, 261–275, doi:10.1029/2000RS002432.

Chang, L. C., C.-H. Lin, J. Yue, J.-Y. Liu, and J.-T. Lin (2013), Stationary planetary wave and nonmigrating tidal signatures in ionospheric wave 3 and wave 4 variations in 2007–2011 FORMOSAT-3/COSMIC observations, *J. Geophys. Res. Space Physics*, *118*, 6651–6665, doi:10.1002/jgra.50583.

Fuller-Rowell, T. J., and D. S. Evans (1987), Height-integrated Pedersen and Hall conductivity patterns inferred from the TIROS-NOAA satellite data, *J. Geophys. Res.*, *92*, 7606–7618, doi:10.1029/JA092iA07p07606.

Fuller-Rowell, T. J., M. V. Codrescu, R. J. Moffett, and S. Quegan (1994), Response of the thermosphere and ionosphere to geomagnetic storms, *J. Geophys. Res.*, *99*, 3893–3914, doi:10.1029/93JA02015.

Hagan, M. E., and J. M. Forbes (2002), Migrating and nonmigrating diurnal tides in the middle and upper atmosphere excited by tropospheric latent heat release, *J. Geophys. Res.*, *107*(D24), 4754, doi:10.1029/2001JD001236.

Hagan, M. E., and R. G. Roble (2001), Modeling diurnal tidal variability with the National Center for Atmospheric Research thermosphere-ionosphere-mesosphere-electrodynamics general circulation model, *J. Geophys. Res.*, *106*, 24,869–24,882, doi:10.1029/2001JA000057.

Hagan, M. E., M. D. Burrage, J. M. Forbes, J. Hackney, W. J. Randel, and X. Zhang (1999), GSWM-98: Results for migrating solar tides, *J. Geophys. Res.*, *104*, 6813–6828, doi:10.1029/1998JA900125.

He, M., L. Liu, W. Wan, J. Lei, and B. Zhao (2010), Longitudinal modulation of the $O/N_2$ column density retrieved from TIMED/GUVI measurement, *Geophys. Res. Lett.*, *37*, L20108, doi:10.1029/2010GL045105.

Hedin, A. E. (1991), Extension of the MSIS thermosphere model into the middle and lower atmosphere, *J. Geophys. Res.*, *96*, 1159–1172, doi:10.1029/90JA02125.

Immel, T. J., E. Sagawa, S. L. England, S. B. Henderson, M. E. Hagan, S. B. Mende, H. U. Frey, C. M. Swenson, and L. J. Paxton (2006), Control of equatorial ionospheric morphology by atmospheric tides, *Geophys. Res. Lett.*, *33*, L15108, doi:10.1029/2006GL026161.

Kil, H., and L. J. Paxton (2011), The origin of the nonmigrating tidal structure in the column number density ratio of atomic oxygen to molecular nitrogen, *Geophys. Res. Lett.*, *38*, L19108, doi:10.1029/2011GL049432.

Luan, X., and X. Dou (2013), Seasonal dependence of the longitudinal variations of nighttime ionospheric electron density and equivalent winds at southern midlatitudes, *Ann. Geophys.*, *31*, 1699–1708, doi:10.5194/angeo-31-1699-2013.

Lühr, H., M. Rother, K. Häusler, B. Fejer, and P. Alken (2012), Direct comparison of nonmigrating tidal signatures in the electrojet, vertical plasma drift and equatorial ionization anomaly, *J. Atmos. Sol. Terr. Phys.*, *75*, 31–43, doi:10.1016/j.jastp.2011.07.009.

Maus, S., et al. (2005), The 10th generation international geomagnetic reference field, *Phys. Earth Planet. Inter.*, *151*, 320–322, doi:10.1016/j.pepi.2005.03.006.

Proelss, G. W. (1980), Magnetic storm associated perturbations of the upper atmosphere—Recent results obtained by satellite-borne gas analyzers, *Rev. Geophys. Space Phys.*, *18*, 183–202, doi:10.1029/RG018i001p00183.

Proelss, G. W. (1981), Latitudinal structure and extension of the polar atmospheric disturbance, *J. Geophys. Res.*, *86*, 2385–2396, doi:10.1029/JA086iA04p02385.

Reigber, C., H. Lühr, and P. Schwintzer (2002), CHAMP mission status, *Adv. Space Res.*, *30*, 129–134.

Ridley, A. J., Y. Deng, and G. Tóth (2006), The global ionosphere thermosphere model, *J. Atmos. Terr. Phys.*, *68*, 839–864.

Rishbeth, H. (1998), How the thermospheric circulation affects the ionospheric F2-layer, *J. Atmos. Terr. Phys.*, *60*, 1385–1402, doi:10.1016/S1364-6826(98)00062-5.

Seaton, M. J. (1956), A possible explanation of the drop in *F*-region critical densities accompanying major ionospheric storms, *J. Atmos. Terr. Phys.*, *8*, 122–124, doi:10.1016/0021-9169(56)90102-7.

Wan, W., J. Xiong, Z. Ren, L. Liu, M. Zhang, F. Ding, B. Ning, B. Zhao, and X. Yue (2010), Correlation between the ionospheric WN4 signature and the upper atmospheric DE3 tide, *J. Geophys. Res.*, *115*, A11303, doi:10.1029/2010JA015527.

Wang, H., H. Lühr, and S. Y. Ma (2005), Solar zenith angle and merging electric field control of field-aligned currents: A statistical study of the Southern Hemisphere, *J. Geophys. Res.*, *110*, A03306, doi:10.1029/2004JA010530.

Weimer, D. R. (2005), Improved ionospheric electrodynamic models and application to calculating Joule heating rates, *J. Geophys. Res.*, *110*, A05306, doi:10.1029/2004JA010884.

Wu, Q., D. A. Ortland, T. L. Killeen, R. G. Roble, M. E. Hagan, H.-L. Liu, S. C. Solomon, J. Xu, W. R. Skinner, and R. J. Niciejewski (2008), Global distribution and interannual variations of mesospheric and lower thermospheric neutral wind diurnal tide: 2. Nonmigrating tide, *J. Geophys. Res.*, *113*, A05309, doi:10.1029/2007JA012543.

Wu, Q., S. C. Solomon, Y. H. Kuo, T. L. Killeen, and J. Y. Xu (2009), Spectral analysis of ionospheric electron density and mesospheric neutral wind diurnal nonmigrating tides observed by COSMIC and TIMED satellites, *Geophys. Res. Lett.*, *36*, L14102, doi:10.1029/2009GL038933.

Wu, Q., W. Wang, R. G. Roble, I. Häggström, and A. Strømme (2012a), First daytime thermospheric wind observation from a balloon-borne Fabry-Perot interferometer over Kiruna (68N), *Geophys. Res. Lett.*, *39*, L14104, doi:10.1029/2012GL052533.

Wu, Q., D. A. Ortland, B. Foster, and R. G. Roble (2012b), Simulation of nonmigrating tide influences on the thermosphere and ionosphere with a TIMED data driven TIEGCM, *J. Atmos. Terr. Phys.*, *90*, 61–67, doi:10.1016/j.jastp.2012.02.009.

Xiong, C., and H. Lühr (2014), The midlatitude summer night anomaly as observed by CHAMP and GRACE: Interpreted as tidal features, *J. Geophys. Res. Space Physics*, *119*, 4905–4915, doi:10.1002/2014JA019959.

Xu, J. S., X. J. Li, Y. W. Liu, and M. Jing (2013), TEC differences for the mid-latitude ionosphere in both sides of the longitudes with zero declination, *Adv. Space Res.*, *54*, 883–895, doi:10.1016/j.asr.2013.01.010.

Zhang, S.-R., J. C. Foster, A. J. Coster, and P. J. Erickson (2011), East-West Coast differences in total electron content over the continental US, *Geophys. Res. Lett.*, *38*, L19101, doi:10.1029/2011GL049116.

Zhang, S.-R., J. C. Foster, J. M. Holt, P. J. Erickson, and A. J. Coster (2012), Magnetic declination and zonal wind effects on longitudinal differences of ionospheric electron density at midlatitudes, *J. Geophys. Res.*, *117*, A08329, doi:10.1029/2012JA017954.

Zhao, B., M. Wang, Y. Wang, Z. Ren, X. Yue, J. Zhu, W. Wan, B. Ning, J. Liu, and B. Xiong (2013), East-west differences in *F*-region electron density at midlatitude: Evidence from the Far East region, *J. Geophys. Res. Space Physics*, *118*, 542–553, doi:10.1029/2012JA018235.